DLS study of a phosphonate induced gypsum scale inhibition mechanism using indifferent nanodispersions as the standards for light scattering intensity comparison

K.I. Popov,[1]* M.S. Oshchepkov,[1,2] N.A. Shabanova,[2] Yu.M. Dikareva,[1] V.E. Larchenko[1] and E. Ya. Koltinova[1]

[1]*PJSC "Fine Chemicals R&D Centre," Krasnobogatyrskaya, 42, str.1, 107258 Moscow, Russian Federation*

[2]*Mendeleev University of Chemical Technology of Russia; 125047, Miusskaya sq. 9, 125047 Moscow, Russian Federation*

**E-mail: ki-popov@mtu-net.ru*

Abstract

The dynamic light scattering (DLS) special technique is used to study the bulk supersaturated gypsum aqueous solutions during the induction period in 0.2 mol·dm^{-3} NaCl at pH 9 and 25°C. It is based on the standard SiO_2 nanoparticles (Ludox TM40) injection into the supersaturated gypsum solution. These nanoparticles act as an internal indifferent light scattering intensity reference and provide a semiquantitative measurement of a relative gypsum particles content in a blank solution and in the system treated with amino-tris(methylenephosphonic acid), ATMP. It is found that ATMP sufficiently reduces the number of gypsum nuclei, spontaneously formed in the supersaturated solutions. In a parallel way the chemical forms of antiscalant in the experimental systems have been modeled. A tentative nonconventional mechanism of scale inhibition is proposed. It assumes that the active crystal formation centers already exist in any analytical grade aqueous solution in the form of solid nanoimpurities with a size ranging from one to several hundred nm. The ATMP antiscalant competes with Ca^{2+} and SO_4^{2-} for these centers and blocks them. Therefore the number of gypsum growth centers diminishes significantly. Thus the concentration of corresponding $CaSO_4 \cdot 2H_2O$ particles gets reduced at least 10-fold. The collision rate of such particles decreases 100-fold. This explains both induction time prolongation by ATMP and sub-stoichiometry of its efficacy.

Received: October 19, 2017. Published: December 15, 2017 doi: 10.17675/2305-6894-2018-7-1-2

Keywords: *stabilization water treatment, gypsum, scale inhibition mechanism, aminotris-(methylenephosphonic acid), DLS, reference nanodispersions.*

1. Introduction

Scaling is a very common problem in boilers and heat exchangers, evaporation plants, RO facilities and oilfield applications [1–4]. A widely used technique for controlling scale deposition is an application of chemical inhibitors [2, 5–8]. Commonly used commercial antiscalants are represented mostly by three chemical families: polyphosphates, organophosphonates and organic polyelectrolytes (polyacrylates (PA), and polycarboxy-sulfonates (PCS)). Among these the organophosphonates are dominating recently at the world market [9]. Irrespective of the broad, successful, and long-term antiscalant applications, the mechanisms of scale inhibition still appear the matter of discussions [10–16].

An excellent recent review [17] summarizes the main steps of scale formation and inhibition mechanisms. The precipitation of a crystalline substance from a solution onto the site of scale formation requires three simultaneous factors: supersaturation, nucleation, and adequate contact time, followed then by the nucleus growth, aggregation, scale deposition and a further growth of the deposit macrocrystals. The inhibitors can alter crystal surface properties and influence the electrical double layers causing changes in nucleation, growth retardation, agglomeration, and crystal morphology.

However, our recent observation of zeta-potentials of $CaCO_3$ and $CaSO_4 \cdot 2H_2O$ scales [18, 19] formed in NACE brines [20] in the presence of conventional inhibitors, reveal that antiscalants do not change the interfacial electrostatic charge values relative to the blank solutions. Moreover, the zeta-potentials for all reagents appear to be insufficient to prevent scale particles aggregation. This result is in a good agreement with an independent study of $CaCO_3$ stabilization by bisphosphonate molecules [16]. Thus, the electrostatic factor is not a universal explanation of an antiscalant efficacy.

At the same time, we have found for a gypsum scale in the NACE brines that the more effective antiscalants do not change the morphology of gypsum, while the less effective one (phosphonobutane-1,2,4-tricarboxylic acid, PBTC) does [19]. As far as the change of the crystal morphology is usually interpreted as a direct approval of the inhibition mechanism, one could expect that the most effective antiscalant should cause the maximal distortion, while the least effective one would reveal the minimal change in the crystal morphology if any. Our observation conflicts this statement. Therefore the supposition that a decreased growth rate of the deposited crystals by blocking the active sites of growth by an antiscalant molecule is also not the case for a particular situation.

Formation of calcium complexes with an antiscalant molecule under a large excess of calcium ions in the systems studied [18, 19] is also an inadequate explanation for scale formation inhibition in NACE brines. In [18, 19] we have supposed that the possible mechanism of scale inhibition in a bulk solution is associated with the reduction of initial number of nucleation centers.

Present study is therefore focused on the dynamic light scattering (DLS) technique application to the bulk supersaturated gypsum aqueous solutions during the induction

period. The latter is denoted as the time between the generation of a supersaturated state and the first observed precipitate. To reach the goal a special measurement technique was elaborated. It is based on the standard nanoparticles injection into the supersaturated gypsum solution. These nanoparticles act as an internal indifferent light scattering intensity reference, and provide a semiquantitative measurement of a relative gypsum particles content in a blank solution and in the system treated with an antiscalant. As far as we know, this is the first report with an estimation of a sparingly soluble salt initial nucleus content.

In a parallel way the chemical forms of antiscalant in the experimental systems have been modeled using a chemical speciation approach for a better understanding of DLS observations.

2. Experimental

2.1 Materials

Analytical grade chemicals were used for brine preparations. Stock solutions of calcium chloride, sodium sulfate, and sodium chloride were prepared from the respective crystalline solids (Aldrich; EKOS-1, Russia) using distilled water. The distilled water, a standard sodium hydroxide aqueous solution, and the final brines were filtered through 0.045 μm Millipore Nylon filters, and then through 0.020 μm filters (Whatman Inorganic membrane filters Anotop 10 Plus). All initial solutions were tested by DLS for the presence of background nanoparticles. It was found that all of them have 1 nm size particles and a much smaller amounts of 200 to 400 nm particles. These exist as impurities in all samples and are characterized by Malvern correlation coefficients from 0.05 to 0.08.

Reagent grade solid aminotris(methylenephosphonic acid) (ATMP; H_6atmp, H_6L) was supplied by a manufacturer OAO "Khimprom", Novocheboksarsk, Russia. Its purity was checked by NMR and then ATMP was used without further purification.

The standard nanodispersions of SiO_2 (Ludox TM40, GRACE Davison) and polystyrene (Malvern) were used as internal references of light scattering intensity. TM40 represents a 45.6% (mass) aqueous solution of SiO_2 sol with an average particle diameter of 40 nm (monomodal) and pH 9. The diluted TM40 sample (0.027 mg·dm^{-3}, pH 9) reveals a zeta-potential within –21 mV. The 0.2 mg·dm^{-3} polystyrene sample demonstrates 300–400 nm particle size (monomodal) with a zeta-potential of –42 mV. Both concentrated dispersions are known to be stable towards aggregation and are capable to keep their initial particle size distribution unchanged for a period ranging from several months to several years.

The desired concentrations of inhibitor and references were obtained by dilution with nanofiltrated deionized water, bearing pH 9 (NaOH).

2.2 Brine and sample preparation

The brines were chosen in such a way that the final gypsum supersaturated solution would have a minimal difference relative to the TM40 reference (pH 9). Two synthetic brines were prepared with distilled water and NaOH: a calcium-containing brine ($CaCl_2 \cdot 2H_2O$, 0.152 mol·dm^{-3} and NaCl, 0.2 mol·dm^{-3}, pH 9) and a sulfate-containing brine (Na_2SO_4, 0.152 mol·dm^{-3} and NaCl, 0.2 mol·dm^{-3}, pH 9). Being mixed at 1:1 volume ratio, these brines give a 0.076 mol·dm^{-3} supersaturated calcium sulfate solution with pH 9 and 0.2 mol·dm^{-3} NaCl. By the end of the precipitation process the ionic strength of this solution was around 0.35 mol·dm^{-3}, provided mostly by NaCl.

According to [21] the solubility of $CaSO_4 \cdot 2H_2O$ in 0.2 mol·dm^{-3} NaCl aqueous solution corresponds to 0.025 mol·dm^{-3} or 4.3 g·dm^{-3} at 25°C. Therefore 0.076 mol·dm^{-3} of gypsum in 0.35 mol·dm^{-3} NaCl at pH 9 and 25°C gives a saturation index SI~3.

In our blank experiments 2 ml of the sulfate brine was mixed with 0.3 ml of distilled water (pH 9) and then 2 ml of calcium brine was added to this mixture. Alternatively, 2 ml of the sulfate brine was mixed with 0.3 ml of ATMP solution (pH 9) and then 2 ml of calcium brine was added to this mixture. This corresponds to 7 mg·dm^{-3} or 0.024 mmol·dm^{-3} content of ATMP in the scale formation system. Then 1 ml of each mixture was sampled and transmitted into the Malvern polystyrene cuvette for DLS measurements. After one and the same period of time (100 or 120 minutes) a portion of 0.025 ml of TM40 was added directly to cuvette with a transparent supersaturated gypsum solution and the DLS measurement immediately started.

2.3 DLS measurements

Liquid phase was monitored by the dynamic light scattering technique. DLS experiments were performed at 25°C with Malvern Nano ZS instrument (λ=633 nm, operating power 4 mW) at Θ=173°. The refractive index n (1.3397), the viscosity η (1123.0 μPa) and the density d (1.062 g·dm^{-3}) of 0.2 mol·dm^{-3} NaCl aqueous solution were measured and used to characterize the solvent. All the brines and antiscalant solutions were clarified by 0.045 μm Millipore Nylon filters to remove dust and checked by DLS technique for the presence of nanoparticles, and then by 0.020 Whatman inorganic membrane filter Anotop 10 Plus. The same operation was done with calcium and sulfate solutions before they were mixed. The samples of saturated calcium sulfate solutions were analyzed for solid phase particle size and ζ-potential. Preliminarily, the reference nanosols (TM40, polystyrene) as well as ATMP solution in the calcium brine were studied. The results are presented in Table 1.

Table 1. The characteristics of internal reference nanodispersions and of ATMP in calcium brine at 25°C.

Dispersion	Fraction Hydrodynamic diameter, nm	Fraction Relative Light Scattering Intensity*, %	Zeta-potential, mV
0.10 mg·dm^{-3} TM40 in an aqueous 0.2 mol·dm^{-3} NaCl solution, pH 9	40±10	100	−21±5
0.20 mg·dm^{-3} polystyrene aqueous solution, pH 9	350±50	100	−42±5
75 mmol·dm^{-3} $CaCl_2 \cdot 2H_2O$ with 0.008 mmol·dm^{-3} ATMP in an aqueous 0.2 mol·dm^{-3} NaCl solution, pH 9	800±200	100	+7±1

* Size distribution by intensity.

2.4 Chemical speciation modeling

Chemical speciation modeling was done using SPECIES software [22] and stability constants from IUPAC DATABASE [23] with data selected for 25° and ionic strength 0–0.3 mol·dm^{-3}. The preference was given to the critically selected IUPAC stability constants [24]. The solubility of sparingly soluble $CaSO_4 \cdot 2H_2O$ [21], $Ca_3(atmp) \cdot 3H_2O$ [25] and $Ca_5(Hatmp)_2 \cdot 5H_2O$ [25] was included as well as the stability constant for the formation of a soluble species $[CaSO_4]^0$ [26].

3. Results and Discussion

3.1 DLS study of indifferent nanosols

Table 1 reveals that the particle sizes of TM40 do not intercept with those of polystyrene. Thus the system TM40/polystyrene was chosen to test the adequacy of relative particle content and relative light scattering intensity. For this purpose, a set of TM40/polystyrene mixture samples with a constant polystyrene content (17 mg·dm^{-3}) and various TM40 concentrations ranging from 0.045 to 0.70 g·dm^{-3} in a constant aqueous solution volume of 1.2 ml at pH 9 were prepared. It was found that the binary sol solutions demonstrate an excellent bimodal size distribution for all the mixtures studied, Figure 1. If not specially specified, the relative integral light scattering intensity *I* (distribution by intensity) was used in the particle size distribution diagrams.

In a binary solution TM40 is indicated as a 40 nm light scattering band, while polystyrene revealed a 350 nm band, as they both have in the individual solutions. At the same time, no aggregation of mixed colloids was observed for at least 24 hours, Figure 2. This experiment proves the high TM40 colloidal stability and its ability to serve as an internal standard.

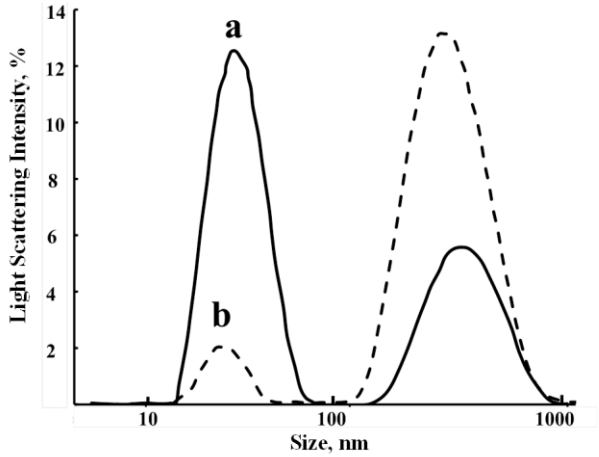

Figure 1. Particle size distribution for the TM40/polystyrene mass ratio 25 (a) and 2.5 (b); SiO_2 is taken as a scattering material.

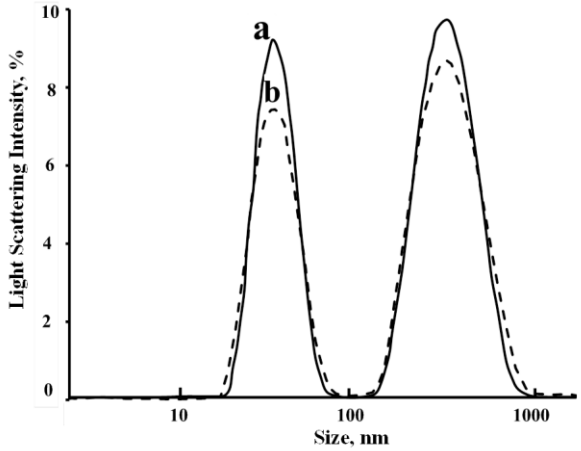

Figure 2. Particle size distribution for the TM40:polystyrene mass ratio 16: 10 minutes (a) and 24 hours after sols mixing (b).

Within the concentration range of diluted TM40 solutions (from 0 to 0.2 $g \cdot dm^{-3}$) an ideal linearity between Ludox relative light scattering intensity and its mass content in a binary colloidal solution was recorded, Figure 3. However, it was not the case for more concentrated solutions, although no aggregation was observed. Thus diluted TM40 solutions (0.027 $g \cdot dm^{-3}$) were chosen for the further experiments with gypsum.

Unfortunately, injection of a reference TM40 sol to the calcium brine in order to estimate the content of heterogeneous impurities was hardly possible, because the high excess of calcium ions enhances the aggregation of TM40 particles. The same problem was found for the ATMP solutions in a calcium brine. However, distilled water (pH 9) and the sulfate brine revealed no interaction with TM40. The "calcium brine – sulfate brine" and "calcium brine – sulfate brine – ATMP" systems after one hour of equilibration demonstrated no interaction with TM40 within at least 30 minutes after its injection.

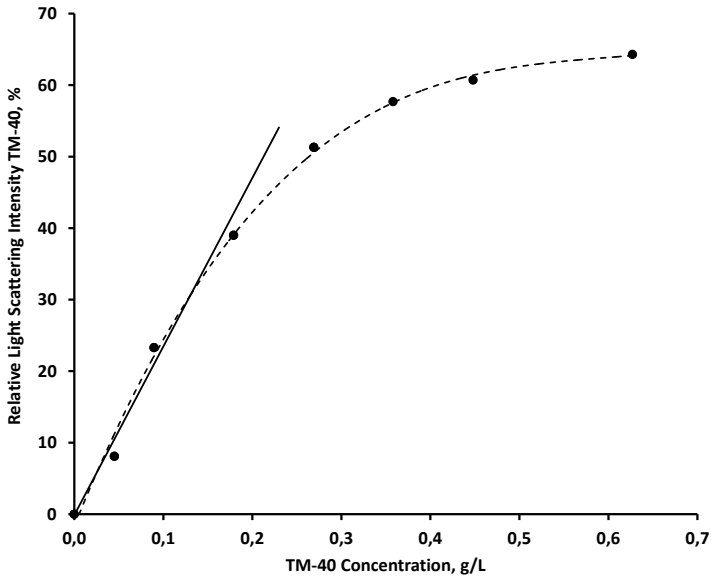

Figure 3. The dependence of TM40 DLS intensity relative to the polystyrene scattering band *versus* the TM40 mass content in the binary colloidal solution.

3.2 Ca–ATMP equilibria study

ATMP is known to form insoluble compounds with calcium ions [24,25,27,28]. Thus it was reasonable to study the binary Ca–ATMP system light scattering under the large excess of calcium ions over ATMP. Figure 4 reveals a fast formation and further growth of big aggregates, which tentatively correspond to $Ca_3(atmp)\cdot 3H_2O$ [25]. Within the first 10 minutes after ATMP injection into the calcium brine the average hydrodynamic particle diameter increases from *ca*. 500 nm to 800–900 nm. However, the solution stays transparent for many days and demonstrates no precipitation, although the zeta-potential of the system is low (+7±1 mV).

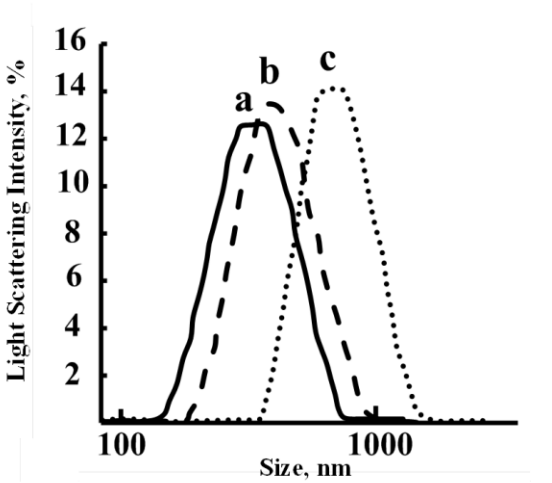

Figure 4. Particle size distribution for the ATMP in calcium brine 2 (a), 5 (b) and 10 (c) minutes after ATMP injection: $[Ca^{2+}]$ = 75 mmol·dm^{-3}; [ATMP] = 0.02 mmol·dm^{-3}; pH 9; 0.2 mol·dm^{-3} NaCl.

This observation is consistent with chemical speciation diagram, Figure 5. Indeed, at pH 9 almost all ATMP molecules exist in the system as insoluble solid form. Only below pH 7 such species as $[CaHL]^{3-}$, $[CaH_2L]^{2-}$ and $[CaH_3L]^{-}$ capable to absorb effectively on a gypsum surface are dominating in the solution.

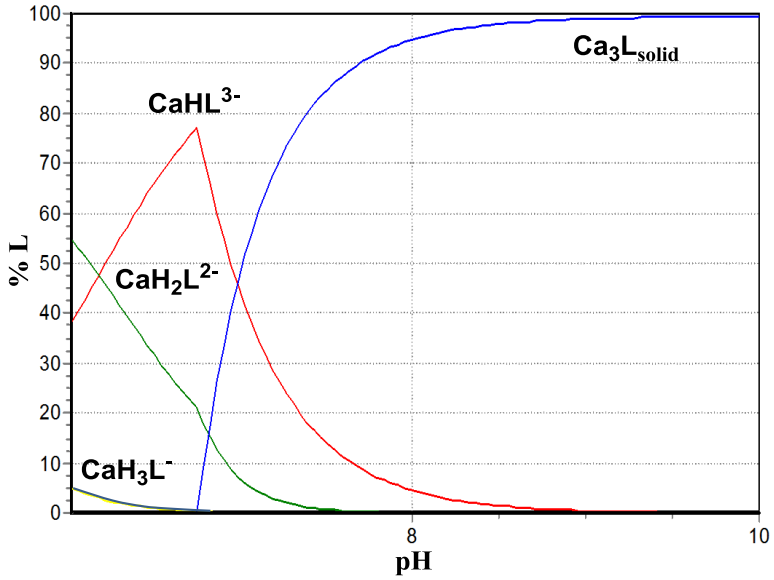

Figure 5. Speciation diagram of ATMP (H_6L) for a binary Ca – ATMP aqueous system, calculated for $[Ca^{2+}]$=75 mmol·dm^{-3}; [ATMP]=0.02 mmol·dm^{-3}; 25°C; 0.2 mol·dm^{-3} NaCl.

The protonated species of Ca–ATMP complexes have been isolated and structurally characterized: $[CaNa_6(Hatmp)_2(H_2O)_{10}][Na(H_2O)_6]_2 \cdot 4H_2O$ [29], $[CaH_4atmp(H_2O)] \cdot 3.5H_2O$ [30, 31]. Both these structures indicate no Ca–N bonding. Therefore the chelate rings are too big to provide effective chelation and high complex stability. However at pH 9 and under a large excess of calcium ions a more stable complex $[CaL]^{4-}$ would dominate in a solution. Its interaction with excessive calcium ions would lead to formation of a sparingly soluble $Ca_3(atmp) \cdot 3H_2O$ salt.

However, in the presence of equimolar amounts of Ca^{2+} and SO_4^{2-} ions almost all calcium concentrates in $CaSO_4 \cdot 2H_2O$ as far as it is less soluble than $Ca_3(atmp) \cdot 3H_2O$. Therefore, according to the speciation model, in a 75 mmol·dm^{-3} gypsum solution at pH 9 ATMP is represented by $[CaHL]^{3-}$ and $[CaL]^{4-}$ species, Figure 6, but not as $Ca_3(atmp) \cdot 3H_2O$.

On the other hand, one should not exclude the formation of $Ca_3(atmp) \cdot 3H_2O$ particles along with $CaSO_4 \cdot 2H_2O$ ones at the first moment of calcium and sulfate brines contact with each other in the presence of ATMP, followed by a slow redistribution of phosphonate forms. However, these Ca–ATMP particles are expected to have negligible light scattering intensity relative to the band of the background $CaSO_4 \cdot 2H_2O$ due to their insignificant mass content in the system studied.

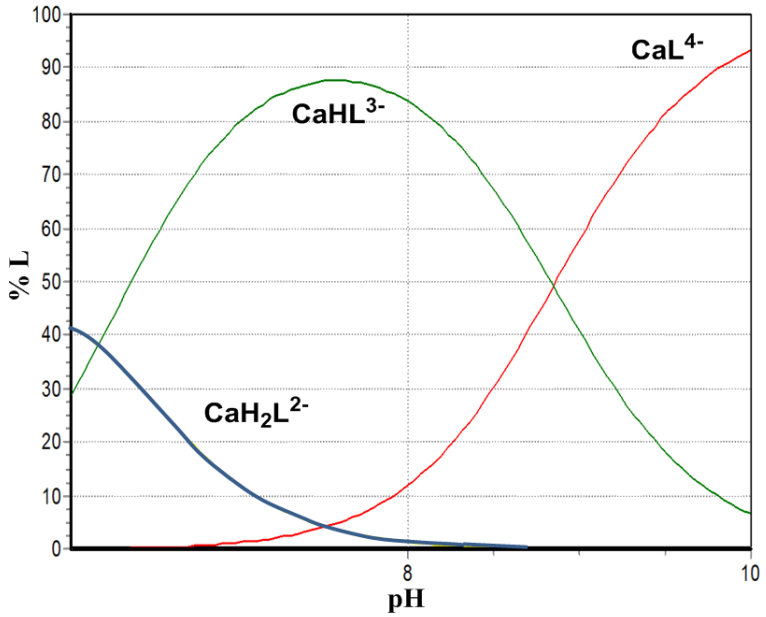

Figure 6. Speciation diagram of ATMP (H_6L) for a gypsum–ATMP aqueous system calculated for $[Ca^{2+}] = [SO_4^{2-}] = 75$ mmol·dm^{-3}; [ATMP] = 0.02 mmol·dm^{-3}; 25°C; 0.2 mol·dm^{-3} NaCl.

3.3 Calcium sulfate supersaturated solutions study

After both calcium and sulfate brines get mixed in an uninhibited (blank) experiment at 25°C, the supersaturated solution remains transparent for 2 to 3 hours, and then some visible small gypsum crystals start to appear in the solution bulk. These crystals grow quickly and form a sediment at the bottom of the glass beaker. Within the first 5 minutes after the brines have contacted each other, DLS indicates the formation of a monomodal fraction with a hydrodynamic diameter (size) of 700±200 nm, Table 2. Within the next 120 minutes the size increases up to *ca*. 800±300 nm and a small fraction of a bigger particle size (~5000 nm) appears. Thus, the formation of big gypsum particles is detected practically immediately after the saturated solution is prepared. However, the bulk liquid phase remains transparent, although the measured zeta-potential of these particles (−12±3 mV) is small and unable to prevent particle aggregation.

Injection of 0.027 g·dm^{-3} TM40 to the blank solution after 120 minutes equilibration results in a separate TM40 band (48±20 nm) and a more intense band of $CaSO_4{\cdot}2H_2O$ (400±150 nm) with a relative gypsum:TM40 scattering intensity ratio of 2.7±0.3, Figure 7a. This ratio and the particle sizes remain constant for 30 minutes, proving that no significant aggregation of TM40 and gypsum takes place. For the sake of clarity, the normalized integral light scattering intensity I_N is used in Figure 7: the TM40 band integral intensity I and its peak intensity are taken equal to unity.

Table 2. The characteristics of gypsum dispersions with TM40 reference added (pH 9, 0.2 mol·dm^{-3} NaCl, 25°C).

Time,* min	$[Ca^{2+}]^0$, mol·dm^{-3}	$[SO_4^{2-}]^0$, mol·dm^{-3}	$ATMP^0$, mmol·dm^{-3}	TM40, g·dm^{-3}	Size, nm	DLS *I*, %	Assignment
5	0.07	0.07	0	0	700±200	100	Gypsum
120	0.07	0.07	0	0	800±300 5300±300	94±2 6±2	Gypsum Gypsum
125	0.07	0.07	0	0.027	48±20 400±150 5300±400	27±2 72±2 1±2	TM40 Gypsum Gypsum
5	0.07	0.07	0.02	0	380±200	100	**
100	0.07	0.07	0.02	0.027	46±10 600±200	88±2 11±3	TM40 **
125	0.07	0.07	0.02	0.027	48±10 550±200	88±2 10±1	TM40 **
1320	0.07	0.07	0.02	0.027	49±10 380±200	87±2 12±1	TM40 **

* Time from the moment the calcium and sulfate brines got mixed.
** Gypsum, or $Ca_3(atmp)\cdot 3H_2O$ or both.

3.4 Calcium sulfate supersaturated solutions in the presence of ATMP study

ATMP was added to the sulfate brine, the mixture equilibrated for 5 minutes under manual shaking, and then the calcium brine was added. In the presence of ATMP (0.02 mmol·dm^{-3} or 7 mg·dm^{-3}) the monomodal fraction of particles with hydrodynamic diameter of *ca.* 400 nm appears immediately in the bulk transparent solution after both calcium and sulfate brines get mixed, Table 2. The measured zeta-potential of these particles (–12±5 mV) is small and unable to prevent the aggregation if particles. Its numerical value is almost the same as in the blank experiment. However, unlike the blank experiment, the supersaturated gypsum solution reveals no crystal formation for more than 1400 minutes.

Injection of 0.027 g·dm^{-3} TM40 to the samples of gypsum inhibited solution taken after 100 and 120 minutes equilibration indicates a separate TM40 band (48±20 nm) and a less intense band, which corresponds to the 600±150 nm particle size fraction, Table 2, Figure 7b. This ratio as well as particle sizes remain constant for 30 minutes, proving that no aggregation of TM40 and gypsum takes place. The relative gypsum:TM40 light scattering intensity ratio after 120 minutes equilibration was found to be much lower than in a blank experiment: 0.10±0.03.

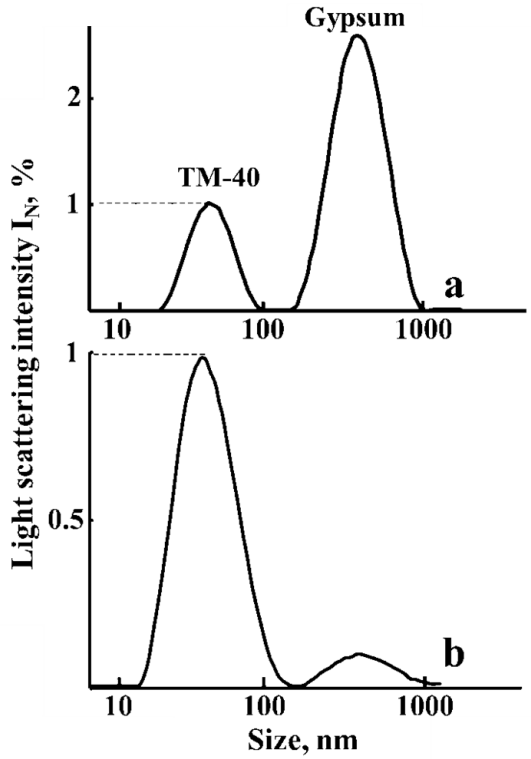

Figure 7. Particle size distribution for the gypsum saturated solution in the presence of 0.027 g·dm^{-3} of TM40 125 minutes after the brines are mixed for uninhibited (a) and inhibited (b) experiments: [Ca^{2+}] = [SO_4^{2-}] = 75 mmol·dm^{-3}; [ATMP] = 0.02 mmol·dm^{-3}; pH 9; 0.2 mol·dm^{-3} NaCl.

An exact origin of 600 nm fraction is hardly possible to identify. It is likely to be gypsum. On the other hand the formation of gypsum and of Ca_3(atmp)·3H_2O mixtures is also possible, although the total ATMP content is c.a. 3000-fold smaller than that of gypsum. The key observation here is that the number of particles formed in an inhibited gypsum solution is evidently one order of magnitude smaller relative to that one present in a blank solution. This result was reproduced in three replicates with gypsum uninhibited/inhibited runs particle content ratio variation from 25 to 10.

As far as we know this is the first report on DLS detection of both an indifferent nano-marker and of the target gypsum nanodispersion. A few communications on DLS application to the scale formation studies refer to $CaCO_3$ nucleation [32, 33], and are all focused on the particle size measurements, but not on their content evaluation. The validity of the marker application is provided by the fact that the gypsum and TM40 particles have different hydrodynamic diameter "windows": 200 to 1000 and 10 to 100 nm respectively. Surely the following conditions should be provided: (i) there should be no interaction of TM40 and gypsum particles right after the marker injection and within the measurement time (5 to 15 minutes); (ii) the gypsum particles relative intensity in an inhibited and uninhibited experiments should be measured at the same time after the moment the brines

get mixed; and (iii) the gypsum particle size in the inhibited and uninhibited experiments should be nearly the same. Our experiment meets all these requirements. Three replicates performed within one week revealed a good agreement. This provides the validity of our approach.

It should be noted that the successful marker application depends on the selection of its proper concentration. Otherwise there is a risk to lose the marker band in the noise of the intensive scale scattering in uninhibited runs, or not to detect scale particles relative to the intensive background scattering of the marker in the inhibited experiments. The chemical nature of the marker is also of great importance. Ludox TM40 used in the present study is not an ideal choice for monitoring of gypsum scaling, as far as it interacts with calcium brine. In order to eliminate this process the marker was injected to the brine mixture one or two hours after they have been mixed, and therefore a significant fraction of calcium was already bound to sulfate ions. Thus the search and selection of more appropriate markers is a matter of future studies.

3.5 Tentative mechanism of gypsum scale formation inhibition by ATMP

A numerical comparison of an inhibited and uninhibited experiment provides some grounds for a nonconventional inhibition mechanism for the case, when two brines are mixed and a supersaturated aqueous solution of a sparingly soluble salt is formed within a very short period of time. All the chemicals available recently for the preparation of such brines ("reagent grade", "puriss.", "extra pure", *etc*.) do not claim the absence of nanoimpurities. In some special purity reagents for microelectronics such impurities are limited to a certain level, but they are still present there. For the majority of others, they are not specified at all. Thus any aqueous solutions prepared from reagent grade chemicals would contain some solid particles of unclear origin. The number of such particles can be partly reduced by nanofiltration, but they cannot be eliminated completely. Indeed, we have registered such particles (*ca.* 1 nm) by DLS as a "noise" in both brines.

Therefore, the formation of gypsum crystals is likely to be enhanced by such nanoimpurities, which serve as the crystallization centers of the $CaSO_4 \cdot 2H_2O$ phase. However, the same nanoimpurities play a similar role in $Ca_3(atmp) \cdot 3H_2O$ formation, or simply do adsorb ATMP molecules. In both cases ATMP "blocks" the surface of such crystallization centers from calcium and sulfate ions, and does not let $CaSO_4 \cdot 2H_2O$ crystals to form. As far as both ATMP and $CaSO_4$ compete for the same set of nanoimpurities, the number of $CaSO_4 \cdot 2H_2O$ nanocrystals gets sufficiently reduced relative to the blank experiment. This is clearly demonstrated in Figure 7.

Assuming that the rate of aggregation corresponds to the second-order kinetics (nanoparticles collision), then the 10-fold decrease in the number of $CaSO_4 \cdot 2H_2O$ particles in the presence of ATMP relative to the blank experiment, leads roughly to a 100-fold decrease in the total aggregation rate. Therefore the 180 to 200 minutes induction time in the blank experiment is expected to be extended by ATMP up to *ca*. 20000 minutes, or to 2 weeks.

Our results partially conflict the conventional theories of the homogeneous scale formation and inhibition in a bulk supersaturated solution. It is widely accepted that the gypsum nucleation is the initial step. Then ATMP gets adsorbed onto gypsum nuclei, thus blocking the active crystal growth sites [3, 5, 10–17, 34–39]. This theoretical ground has stimulated numerous studies on selection of inhibitors that are better adsorbed onto gypsum, calcite or another scale to form a solid surface [39–44].

Our data reveal a somewhat different situation. The active crystal formation centers do already exist in any analytical grade aqueous solution in the form of solid nanoimpurities with a size ranging from one to several hundred nm. The particle concentration of these nanoimpurities is likely to be comparable with the molar concentrations of the antiscalant used. Surely these impurities are much better represented in tap water or in industrial cooling water. In supersaturated gypsum aqueous solutions, particularly these nanoimpurities act as $CaSO_4 \cdot 2H_2O$ crystal formation centers. Indeed, we have observed the fast formation of the 500–800 nm particle fraction with a low zeta-potential in a blank experiment, which slowly underwent further aggregation to form 4000 to 5000 nm aggregates, followed by their precipitation within a couple of hours.

The ATMP antiscalant competes with Ca^{2+} and SO_4^{2-} for these indifferent centers and blocks them. Therefore the number of gypsum growth centers diminishes significantly. Thus the concentration of the corresponding $CaSO_4 \cdot 2H_2O$ particles gets reduced 10-fold. The collision rate of such particles decreases 100-fold. This explains both the induction time prolongation by ATMP and the sub-stoichiometry of its efficacy.

4. Conclusions

The conclusions drawn from this study are as follows:

1) The application of a proper indifferent nanodispersion as an internal standard of particle concentration in DLS scale inhibition experiments is feasible. Ludox TM40 may be used for the gypsum nucleation monitoring in supersaturated solutions at pH 9.
2) It is found that ATMP sufficiently reduces the number of gypsum nuclei formed in supersaturated solutions.
3) A tentative mechanism of scale inhibition is proposed. The active crystal formation centers already exist in any analytical grade aqueous solution in the form of solid nanoimpurities with a size ranging from one to several hundred nm. The ATMP antiscalant competes with Ca^{2+} and SO_4^{2-} for these centers and blocks them. Therefore the number of gypsum particles diminishes significantly. Thus the rate of further aggregation of gypsum nuclei gets reduced sufficiently.

Acknowledgement

The authors would like to thank the Russian Foundation for Basic Research (Project No. 17-08-00061) for the financial support of the present study.

References

1. J. MacAdam and P. Jarvis, "Water-Formed Scales and Deposits: Types, Characteristics, and Relevant Industries," in *Mineral Scales and Deposits*, *Scientific and Technological Approaches,* eds. Z. Amjad and K. Demadis, 1st Edition Scientific, Elsevier, 2015, pp. 3–23.
2. K.I. Popov, N.E. Kovaleva, G.Ya. Rudakova, S.P. Kombarova and V.E. Larchenko, "Recent State-of-the-Art of Biodegradable Scale Inhibitors for Cooling Water Treatment Applications (Review)", *Therm. Eng.*, 2016, **63**, 122–129.
3. A.A. Olajire, "A review of oilfield scale management technology for oil and gas production", *J. Pet. Sci. Eng*., 2015, **135**, 723–737.
4. A. Antony, J.H. Low, S. Gray, A.E. Childress, P. Le-Clech and G. Leslie, "Scale formation and control in high pressure membrane water treatment systems: A review", *J. Membr. Sci.*, 2011, **383**, 1–16.
5. Z. Amjad, "Kinetic and morphological investigation of calcium sulfate dihydrate (gypsum) scale formation on heat exchanger surfaces in the presence of inhibitors", *Int. J. Corros. Scale Inhib.*, 2017**, 6**, no. 3, 276–290. doi: 10.17675/2305-6894-2017-6-3-4
6. Z. Amjad, R.T. Landgraf and J.L. Penn, "Calcium sulfate dihydrate (gypsum) scale formation by PAA, PAPEMP, and PAA/PAPEMP blend", *Int. J. Corros. Scale Inhib*., 2014, **3**, no. 1, 35. doi: 10.17675/2305-6894-2014-3-1-035-047
7. X. Li, H. Shemer, D. Hasson and R. Semiat, "Characterization of the effectiveness of anti-scalants in suppressing scale deposition on a heated surface", *Desalination*, 2016, **397**, 38–42.
8. K.D. Demadis and M. Preari, "Green" scale inhibitors in water treatment processes: the case of silica scale inhibition", *Desalin. Water Treat*., 2015, **55**, 749–755.
9. Scale Inhibitor Market by Type and by Application – Global Trends & Forecast to 2019 / http://www.researchandmarkets.com/reports/2933881/scale-inhibitormarket-by-type-and-by-application#pos-0.
10. M.N. Elliott, "Scale control by threshold treatment", *Desalination*, 1970, **8**, 221–236.
11. M.M. Reddy and G.H. Nancollas, "Calcite crystal growth inhibition by phosphonates", *Desalination*, 1973, **12**, 61–73.
12. B.M. Tomson, G. Fu, M.A. Watson and A.T. Kan, "Mechanisms of mineral scale inhibition", *SPE Prod. Facil.*, 2003, **18**, 192–199.
13. G. Zhang, J. Ge, M. Sun, B. Pan, T. Mao and Z. Song, "Investigation of scale inhibition mechanisms based on the effect of scale inhibitor on calcium carbonate crystal forms", *Sci. China, Ser. B: Chem*., 2007, **50**, 114–120.
14. L. Liu and A. He, "Research progress of scale inhibition mechanism"**,** *Adv. Mater. Res*., 2014, **955–959**, 2411–2414.
15. Y.M. Al-Roomi and K.F. Hussain, "Potential kinetic model for scaling and scale inhibition mechanism", *Desalination*, 2016, **393**, 186–195.

16. J. Ge, W. Yang, G. Zhang, J. Ping and M. Sun, "Investigation of scale inhibition mechanisms based on the effect of HEDP on surface charge of calcium carbonate", *Tenside, Surfactants, Deterg.*, 2016, **53**, 29–36.
17. T.A. Hoang, "Mechanisms of Scale Formation and Inhibition", in *Mineral Scales and Deposits*, *Scientific and Technological Approaches,* eds. Z. Amjad and K. Demadis, 1st Edition, Elsevier, 2015, pp. 47–83.
18. K. Popov, G. Rudakova, V. Larchenko, M. Tusheva, E. Afanas'eva, S. Kombarova, S. Kamagurov and N. Kovaleva, "A comparative performance ranking of some phosphonates and environmentally friendly polymers on $CaCO_3$ scaling inhibition by NACE protocol", *Desalin. Water Treat.*, 2017, **69,** 163–172.
19. K. Popov, G. Rudakova, V. Larchenko, M. Tusheva, S. Kamagurov, J. Dikareva and N.A. Kovaleva, "Comparative Performance Evaluation of Some Novel 'Green' and Traditional Antiscalants in Calcium Sulfate Scaling", *Adv. Mater. Sci. Eng.*, 2016, **2016**, Article ID 7635329, 10 pp.
20. NACE Standard TM0374-2007 (formerly TM0374-2001), Item No. 21208, Laboratory Screening Tests to Determine the Ability of Scale Inhibitors to Prevent the Precipitation of Calcium Sulfate and Calcium Carbonate from Solution (for Oil and Gas Production Systems), 2007.
21. K. Raju and G. Atkinson, "The thermodynamics of «scale» mineral solubilities. 3. Calcium sulfate in aqueous sodium chloride", *J. Chem. Eng. Data*, 1990, **35**, 361–367.
22. R. Byrne, T. Kiss, L. Lövgren, P.M. May, C.O. Onindo, L.D. Pettit, K.I. Popov, K.J. Powell, R.W. Ramette, S. Sjöberg; R.M. Town and L.O. Ohman, *SPECIES in Solution Equilibria: Principles and Applications [Windows 95, 98]*, Academic Software and K.J. Powell, Release 1.04, 2000 (SolEq).
23. *Stability Constants Database and Mini-SCDatabase*, IUPAC and Academic Software, Version 5.3, 2011, Sourby Old Farm, Timble, Otley, Yorks, UK; scdbase@acadsoft.co.uk.
24. K.I. Popov, H. Rönkkömäki and L.H.J. Lajunen, "Critical Evaluation of Stability Constants of Phosphonic Acids", *Pure Appl. Chem.*, 2001, **73**, 1641–1677.
25. N.M. Dyatlova, V.Ya. Temkina and K.I. Popov, *Kompleksony i kompleksonaty metallov (Complexones and Complexonates of Metals)*, Moscow, Khimiya, 1988, 544 pp. (in Russian).
26. F.H. Fisher and A.P. Fox, "Divalent sulfate ion pairs in aqueous solutions at pressures up to 2000 atm", *J. Solution Chem.*,1979, **8**, 309–328.
27. R. Pairat, C. Sumeath, F.H. Browning and H.S. Fogler, "Precipitation and Dissolution of Calcium – ATMP Precipitates for the Inhibition of Scale Formation in Porous Media", *Langmuir*, 1997, **13**, 1791–1798.
28. B.R. Zhang, L. Zhang, F.T. Li, W. Hu and P.M. Hannam, "Testing the formation of Ca-phosphonate precipitates and evaluating the anionic polymers as Ca-phosphonate precipitates and $CaCO_3$ scale inhibitor in simulated cooling water", *Corros. Sci.*, 2010, **52**, 3883–3890.

29. N.V Somova, F.F. Chausov and R.M. Zakirovac, "Synthesis and Structure of Decaaqua-Hexasodium-Calcium Bis-nitrilotris(methylenephosphonate) Bis(hexa-aquasodium) Tetrahydrate $[CaNa_6\{NH(CH_2PO_3)_3\}_2(H_2O)_{10}][Na(H_2O)_6]_2 \cdot 4H_2O$", *Crystallogr. Rep.*, 2017, **62**, 397–404.
30. N. Stavgianoudaki, K.E. Papathanasiou, R.M.P. Colodrero, D. Choquesillo-Lazarte, J.M. Garcia-Ruiz, A. Cabeza, M.A.G. Aranda and K.D. Demadis, "Crystal Engineering in Confined Spaces. A Novel Method to Grow Crystalline Metal Phosphonates in Alginate Gel Systems", *CrystEngComm.*, 2012, **14**, 5385–5389.
31. K.D. Demadis and S.D. Katarachia, "Metal-Phosphonate Chemistry: Preparation, Crystal Structure of Calcium-Amino*tris(*Methylene Phosphonate) and $CaCO_3$ Inhibition", *Phosphorus, Sulfur Silicon Relat. Elem.*, 2004, **179**, no. 3, 627–648.
32. M.F.B. Sousa and C.A. Bertran, "New methodology on static light scattering measurements for evaluation of inhibitors for in bulk $CaCO_3$ crystallization", *J. Colloid Interface Sci*., 2014, **420**, 57–64.
33. M. Dietzsch, I. Andrusenko, R. Branscheid, F. Emmerling, U. Kolb and W. Tremel, "Snapshots of calcium carbonate formation – a step by step analysis", *Z. Kristallogr. – Cryst. Mater.*, 2016, **232**, 255–265.
35. F. Rahman, "Calcium sulfate precipitation studies with scale inhibitors for reverse osmosis desalination", *Desalination*, 2013, **319**, 79–84.
36. M. Gloede and T. Melin, "Potentials and limitations of molecular modeling approaches for scaling and scale inhibiting mechanisms", *Desalination*, 2006, **199**, 26–28.
37. G.H. Nancollas, W. White, F. Tsai and L. Maslow, "The kinetics and mechanism of formation of Calcium Sulfate scale minerals – The Influence of inhibitors", *Corrosion*, 1979, **35**, 304–308.
38. L. Liu and A. He, "Research progress of scale inhibition mechanism" *Adv. Mater. Res*., 2014**, 955–959**, 2411–2414.
39. E. Akyol, M. Öner, E. Barouda and K.D. Demadis, "Systematic Structural Determinants of the Effects of Tetraphosphonates on Gypsum Crystallization", *Cryst. Growth Des*., 2009, **9**, 5145–5154.
40. X. Li, D. Hasson and H. Shemer, "Flow conditions affecting the induction period of $CaSO_4$ scaling on RO membranes", *Desalination*, 2017, *Ahead of Print*.
41. N. Xu, M. Chen, K. Zhou, Y. Wang, H. Yin and Z. Chen, "Retention of Phosphorus on Calcite and Dolomite: speciation and modeling", *RSC Adv.*, 2014, **4**, 35205–35214.
42. M.P.C. Weijnen and G.M. van Rosmalen, "Adsorption of phosphonates on gypsum crystals", *J. Cryst. Growth,* 1986, **79**, 157–168.
43. A.T. Kan, G. Fu and M.B. Tomson, "Adsorption and precipitation of aminoalkyl-phosphonate onto calcite", *J. Coll. Interface Sci*., 2005, **281**, 275–284.
44. S.T. Liu and G.H. Nancollas, "The crystal growth of calcium sulfate dihydrate in the presence of additives", *J.Coll. Interface Sci.,* 1973, **44**, 422–429.

♦ ♦ ♦